In Vivo Imaging of Tumor-Propagating Cells, Regional Tumor Heterogeneity, and Dynamic Cell Movements in Embryonal Rhabdomyosarcoma

Myron S. Ignatius,[1,3] Eleanor Chen,[1,3,4] Natalie M. Elpek,[2] Adam Z. Fuller,[1,3] Inês M. Tenente,[1,3,5] Ryan Clagg,[1,3] Sali Liu,[1,3] Jessica S. Blackburn,[1,3] Corinne M. Linardic,[6] Andrew E. Rosenberg,[1] Petur G. Nielsen,[1] Thorsten R. Mempel,[2] and David M. Langenau[1,3,*]

[1]Department of Pathology and Center for Cancer Research
[2]Center for Immunology and Inflammatory Diseases
Massachusetts General Hospital, Charlestown, MA 02129, USA
[3]Harvard Stem Cell Institute, Boston, MA 02114, USA
[4]Department of Pathology, Brigham and Women's Hospital, Boston, MA 02115, USA
[5]Instituto de Ciências Biomédicas Abel Salazar, 4099-003 Porto, Portugal
[6]Departments of Pediatrics, Pharmacology, and Cancer Biology, Duke University Medical Center, Durham, NC 27710, USA
*Correspondence: dlangenau@partners.org
DOI 10.1016/j.ccr.2012.03.043

SUMMARY

Embryonal rhabdomyosarcoma (ERMS) is an aggressive pediatric sarcoma of muscle. Here, we show that ERMS-propagating potential is confined to *myf5+* cells and can be visualized in live, fluorescent transgenic zebrafish. During early tumor growth, *myf5+* ERMS cells reside adjacent normal muscle fibers. By late-stage ERMS, *myf5+* cells are reorganized into distinct regions separated from differentiated tumor cells. Time-lapse imaging of late-stage ERMS revealed that *myf5+* cells populate newly formed tumor only after seeding by highly migratory *myogenin+* ERMS cells. Moreover, *myogenin+* ERMS cells can enter the vasculature, whereas *myf5+* ERMS-propagating cells do not. Our data suggest that non-tumor-propagating cells likely have important supportive roles in cancer progression and facilitate metastasis.

INTRODUCTION

Rhabdomyosarcoma (RMS) is a pediatric malignancy that shares common features with skeletal muscle arrested in embryonic development (Xia et al., 2002). The two main subtypes of pediatric rhabdomyosarcoma, embryonal RMS (ERMS) and alveolar RMS (ARMS), differ in their clinical, biological, and molecular characteristics. For example, ERMS and ARMS can be distinguished based on histology and have different long-term prognoses, with ERMS patients having better overall outcome than ARMS patients. These divergent clinical features likely reflect the use of different molecular programs that lead to transformation. For example, we have identified that the RAS pathway is active in a majority of human ERMS (Hettmer et al., 2011; Langenau et al., 2007). By contrast, 85% of ARMS cells have recurrent chromosomal translocations that juxtapose PAX3 or PAX7 with the forkhead transcription factor (FKHR) (Xia et al., 2002). Finally, it is likely that ERMS and translocation-positive ARMS arise in different cell types that eventually undergo transformation. Keller et al. (2004) found that PAX3-FKHR+ ARMS can arise from Myf6-expressing myoblast cells but not dermamyotome or satellite cells that express Pax7. By contrast, ERMS can arise from either satellite cells or myoblasts that eventually reinitiate molecular programs found in satellite cells (Rubin et al., 2011). Despite elegant studies defining possible cells of origin in RMS, identification of an ERMS-propagating cell that is required for continued tumor growth in vivo has not been described in mice or humans.

Significance

Tumor-propagating potential is not found in all malignant cells, and, in most cancers, cells with more differentiated features are largely incapable of remaking tumor and yet constitute a majority of the tumor mass. A role for differentiated malignant cells in tumor growth, including dissemination and metastasis, has not been fully explored. We find that mid-differentiated *myogenin*-positive ERMS cells lack tumor-propagating potential yet are responsible for local invasion and can enter the vasculature. Slow-moving *myf5+* ERMS-propagating cells are recruited to new sites of tumor growth after seeding by differentiated ERMS cells. This finding may explain the clinical observation that Myogenin positivity correlates with poor clinical outcome in human ERMS and suggests that differentiated tumor cells play critical roles in metastasis.

Tumor-propagating cells have been characterized in many malignances, and in some tumors, this potential is confined to a molecularly definable cell population that can be enriched by cell surface markers. For example, in acute myeloid leukemia, a rare CD34$^+$CD38$^-$ cell enriches for leukemia-propagating potential while in breast cancer CD44$^+$CD24$^{low/-}$ expression is associated with tumor-propagating potential (reviewed in Dalerba et al., 2007). Molecularly defined, rare CD133$^+$ tumor-propagating cells have also been identified in a subset of gliomas and exhibit striking differences in response to nitric oxide and hypoxia inducible factor signaling when compared to more differentiated tumor cells (Eyler et al., 2011; Li et al., 2009). Thus, it is likely that many tumors contain hierarchically organized cell subpopulations that retain the capacity to remake tumor and yet give rise to differentiated tumor cell progeny. One might expect that selection would favor the evolution of tumors with high numbers of tumor-propagating cells at a cost of differentiated cell types. Paradoxically, however, in most malignancies, tumor-propagating cells are far less abundant than differentiated tumor cells that are incapable of remaking tumor. These data suggest that differentiated tumor cells may provide important supportive roles in overall growth and maintenance. To date, a role for differentiated, non-tumor-propagating ERMS cells has yet to be fully explored.

Stem cells often reside in distinct niches in normal tissue, and their functions are exquisitely controlled by local factors secreted by supporting cells. For example, hematopoietic stem cells (HSCs) have been shown to home to niches within the calvarium that are tightly associated with osteoblasts (Lo Celso et al., 2009). These and other niche-associated cells presumably provide paracrine-signaling factors to recruit and maintain these cells in a specific niche. Unlike other tissues, the muscle stem cell niche is defined by juxtaposition of satellite cells next to differentiated muscle fibers, and their numbers and differentiation capacity are controlled by complex signaling pathways regulated by mature muscle cells (reviewed in Bentzinger et al., 2012). Despite a large body of data defining stem cell niches in normal tissue, few studies have identified tumor-specific niches and/or regions of compartmentalized tumor cell function and fewer still have used microscopic imaging to directly visualize tumor-propagating cells within live animals. In one example, Sipkins et al. (2005) used a combination of multiphoton and confocal microscopy to image the HSC niche in the calvarium of mice and demonstrated that these sites can attract multiple tumor cell types; however, it is unknown if these malignant cells are capable of reinitiating tumors. In ERMS, as with most solid tumors, it is unknown whether tumor-propagating cells reside in distinct regions within the tumor mass and whether the more differentiated cells play a role in promoting tumor progression.

Here, we utilize a transgenic zebrafish model of ERMS to identify the tumor-propagating cell in this disease and to define the functional consequences of tumor cell heterogeneity within live animals. Because ERMS cell subpopulations can be fluorescent labeled based on myogenic factor expression, ERMS cell subtypes can be visualized in live animals and the processes of cell growth, division, and local dissemination can be visualized as dynamic processes in live animals. Our data provide an explanation for the large number of non-tumor-propagating cells in established cancers and reveal an important supportive role for differentiated tumor cell types in local dissemination and metastasis.

RESULTS

Imaging Distinct Stages of ERMS Growth

Externally visible ERMS can develop as early as 10 days of life in zebrafish injected with *rag2-KRASG12D* (Langenau et al., 2007), and >80% of ERMS develop in the tail musculature (n > 50). To assess how tumors initiate and evolve in zebrafish ERMS, we injected *α-actin-GFP* transgenic zebrafish at the one-cell stage of development with *rag2-dsREDexpress* and *rag2-KRASG12D* (Figures 1A–1F), facilitating imaging of ERMS cells in relation to normal muscle. Microinjection of multiple transgenes into one-cell-stage animals leads to cointegration and coexpression in animals that develop ERMS (Langenau et al., 2008). This approach provides a robust method to create mosaic transgenic animals with fluorescently labeled ERMS cell subpopulations (Langenau et al., 2007).

Sequential confocal imaging over several days showed that ERMS forms in a choreographed and stereotypical manner (Figures 1A–1F and 1J–1M). Specifically, dsRed+ ERMS mononuclear cells arise at the extreme outer borders of the myotome segments and move toward the midline where they are initially unable to bypass the horizontal myosepta—a single cell layer that separates myotome segments (Figure 1A; stage 1, n = 7). After several days, a subset of cells cross the horizontal myosepta and take up residence between normal muscle fibers within the newly colonized myotome segment (stage 2; Figures 1B and 1C; n = 5). Differentiated ERMS cells that express both *rag2-dsREDexpress* and *α-actin-GFP* can move laterally into neighboring muscle segments by transiting through the collagen matrix of the myoseptum (n = 6; Figures 1D–1F; Movie S1 available online) or stream into new myotome segments by growing past the edge of myoseptum (n = 3, early stage 3). The collagen matrix of the muscle myoseptum is a cell-impermeable barrier that is the site of muscle attachment in teleost fish and is similar in function to tendons in mouse and humans. Late-stage ERMS cells undergo rapid loss of fibers, breakdown of normal muscle architecture including collagen remodeling, and development of mononuclear tumor cells, reminiscent of the spindle variant of human ERMS.

Neovascularization is a hallmark of cancer and an ideal surrogate for assessing tumorigenicity. To assess when KRASG12D-expressing cells are transformed, we monitored neovascularization in *fli1-GFP* transgenic animals that were injected at the one-cell stage of life with *rag2-KRASG12D* and *rag2-dsREDexpress*. Animals were monitored for tumor growth by confocal microscopy beginning at 10 days of life (n = 22; Figures 1G–1I). ERMS at stage 1 failed to recruit new vasculature (n = 0 of 3), but stage 2 and early stage 3 ERMS had begun to recruit new vasculature (n = 8 of 8; Figure 1H) with new branches arising from both the intersegmental vessels and vertebral artery. By late stage 3, ERMS developed intricate networks of new vessels (n = 11 of 11; Figure 1I). Our imaging studies define distinct stages of ERMS growth and suggest that RAS-expressing cells become fully transformed by stage 2 of tumor development (Figures 1J–1M).
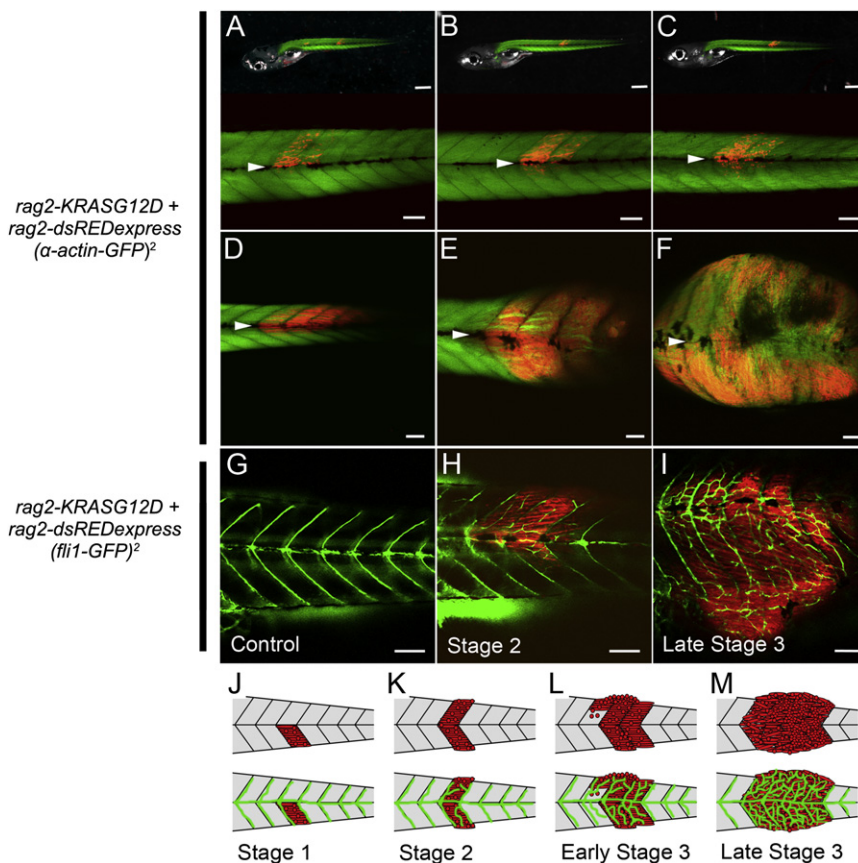
Figure 1. Visualizing Distinct Stages of Embryonal RMS Growth

(A–F) *rag2-dsRED*-labeled ERMS arising in *α-actin-GFP* transgenic zebrafish. The same animal imaged at 6, 9, and 12 days postfertilization (dpf) is shown in (A), (B), and (C), respectively. A representative zebrafish where dsRED+ ERMS cells have already bypassed the horizontal myoseptum and migrated into new segments that were previously free of tumor (F, stage 3) at 13, 18, and 24 dpf is shown in (D), (E), and (F), respectively. The horizontal myoseptum is denoted by white arrows.

(G–I) *fli1-GFP* transgenic control animal (G) compared with a *rag2-dsRED*-labeled ERMS arising in *fli1-GFP* transgenic zebrafish at early stage 2 (H) or a late stage 3 (I).

(J–M) Schematic of stages of ERMS growth.

Scale bars in the upper panels of (A) through (C), 500 μm. Scale bars in the lower panels of (A) through (C) and in (D) through (I), 100 μm.

See also Movie S1.

Identification of Molecularly Distinct Fluorescent-Labeled ERMS Cell Subpopulations

Previous experiments in zebrafish have identified an ERMS cell subpopulation that had superior tumor-propagating potential when compared to other tumor-derived cells. This ERMS-propagating cell was *rag2-dsREDexpress+/α-actin-negative* and expressed high levels of *myf5*, *c-met*, and *m-cadherin*—markers of satellite and early muscle progenitor cells (Langenau et al., 2007). *MYF5* is highly upregulated in human ERMS compared to both translocation positive ARMS and normal muscle (Zibat et al., 2010) and in comparing zebrafish ERMS to normal muscle (Langenau et al., 2007). To directly assess whether *myf5* labels distinct ERMS cell subpopulations, *myf5-GFP/myosin light chain 2-mCherry* (*mylz2*) syngeneic animals were created by four rounds of outcrossing to CG1 syngeneic animals (Smith et al., 2010) and injected at the one-cell stage with *rag2-KRASG12D*. *myf5*-GFP transgenic animals exhibit green fluorescent protein (GFP) expression in early somitogenesis and later in satellite cells and early muscle progenitor cells (Chen et al., 2007; Seger et al., 2011) while the *mylz2* promoter drives expression in differentiated muscle cells (Ju et al., 2003; Smith et al., 2010). Fluorescent-labeled ERMS cell subpopulations were isolated from double transgenic animals by fluorescence-activated cell sorting (FACS). Reanalysis of sorted cells by FACS confirmed that ERMS contained four distinct populations of cells (purity > 87% and viability > 97%).

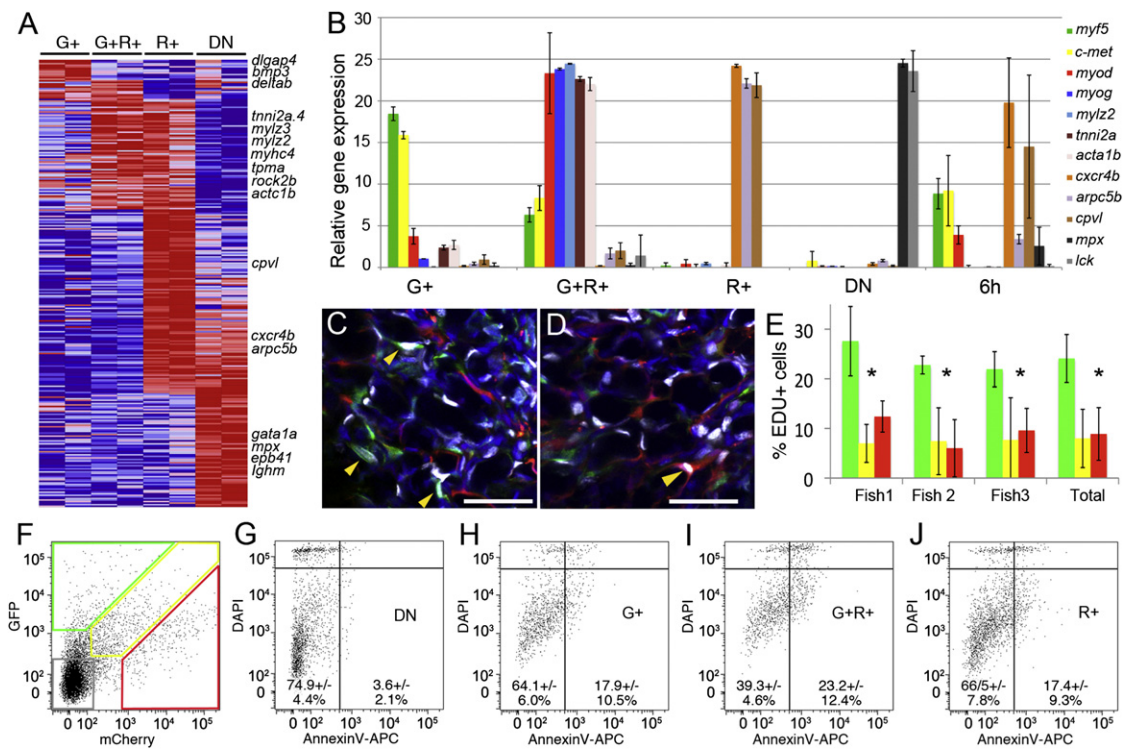To verify that discrete fluorescent-labeled ERMS cell subpopulations were molecularly distinct, sorted cell populations were assessed for gene expression differences based on microarray (Figure 2A; Table S1) and real-time PCR (Figures 2B and S1). Gene expression analysis was completed on FACS-sorted ERMS cells derived from serially passaged tumors, ensuring that fluorescent-labeled cells were tumor derived. Microarray analysis confirmed that each cell subpopulation exhibited wide differences in gene expression. Subsequent real-time PCR analysis established that the *myf5-GFP+/mylz2-mCherry-negative* cells expressed high levels of *myf5*, *c-met*, and *m-cadherin* but not *pax7a*, *pax7b*, or differentiated markers (Figures 2B and S1). By contrast, *mylz2-mCherry+* ERMS cells expressed high levels of mature muscle markers including *myod*, *myogenin*, *troponin I fast-twitch isoform 2* (*tnni2a*), *α-actin 1b* (*acta1b*), *ventricular myosin heavy chain-like* (*vmhcl*), *actin-related protein 2/3 complex subunit 5B* (*arpc5b*), *carboxypeptidase vitellogenic-like* (*cpvl*), and *chemokine (C-X-C motif) receptor 4b* (*cxcr4b*). Finally, the double-negative cell population comprised predominantly blood cells that express *myeloid-specific peroxidase* (*mpx*) and *lymphocyte-specific protein tyrosine kinase* (*lck*). Our data confirm that fluorescent-labeled ERMS cell subpopulations can be prospectively isolated to relative purity following FACS and are molecularly distinct.

Given that FACS could identify unique ERMS cell subpopulations that exhibited wide differences in gene expression, we questioned whether these cells also differ in rates of proliferation and cellular turnover. Proliferation was assessed at 6 hr following intraperitoneal injection of EDU into ERMS-affected animals (Figures 2C–2E and S1). *myf5-GFP+/mylz2-mCherry-negative* cells (24.1% ± 4.8%) incorporated EDU over a 6 hr pulse, whereas differentiated ERMS cells that express *mylz2-mCherry* were far less proliferative (8.9% ± 5.0%; p < 0.00001). By contrast, following 3-day administration of EDU, all fluorescent-labeled ERMS cell subfractions exhibited equal proliferative capacity, suggesting that *myf5-GFP+/mylz2-mCherry-negative*

Figure 2. Fluorescent Transgenic Approaches Identify Discrete and Molecularly Definable ERMS Cell Subpopulations in *myf5-GFP/mylz2-mCherry* Transgenic Fish

(A) Heat map showing differential gene expression between FACS-sorted ERMS cell subpopulations isolated from serially passaged *myf5-GFP/ mylz2-mCherry* ERMS (microarray log fold-change > 1.5). *myf5-GFP+/mylz2-mCherry-negative* (G+), *myf5-GFP+/mylz2-mCherry+* (G+R+), *myf5-GFP-negative/mylz2-mCherry+* (R+), and double negative (DN).

(B) Quantitative real-time PCR of sorted ERMS cell subpopulations. Expression values, ±1 SD.

(C and D) Confocal images of EDU-stained sections from serially passaged *myf5-GFP+/mylz2-mCherry+* ERMS. Tumor regions with large numbers of either *myf5-GFP+* (C) or *mylz2-mCherry+* ERMS cells (D). Blue denotes DAPI+ nuclei, and white denotes EDU+ nuclei. Yellow arrows indicate EDU-labeled cells. Scale bar, 25 μm.

(E) Quantification of EDU incorporation over a 6 hr EDU pulse. Data for *myf5-GFP+/mylz2-mCherry-negative* ERMS cells are denoted by green bars, data for *myf5-GFP+/mylz2-mCherry+* cells are indicated by yellow bars, and data for *myf5-GFP-negative/mylz2-mCherry+* cells are indicated by red bars. Three individual tumors shown as well as cumulative data across all tumors (Total). *p < 0.00001. Error bars, ±1 SD.

(F) FACS plot of serially passaged *myf5-GFP/mylz2-mCherry* ERMS.

(G–J) Gated ERMS cells assessed for DAPI and AnnexinV-APC staining (double negative, DN) (G); *myf5-GFP+/mylz2-mCherry-negative* (G+) (H); *myf5-GFP+/ mylz2-mCherry+* (G+R+) (I); and *myf5-GFP-negative/mylz2-mCherry+* (R+) (J). Live cells are shown within the DAPI-negative/AnnexinV-negative gates.

See also Figure S1 and Table S1.

cells divided and differentiated over this time (data not shown). In addition to striking differences in cell proliferation between ERMS cell subpopulations, *myf5-GFP+/mylz2-mCherry+* cells had higher levels of apoptotic cellular turnover when compared with *myf5-GFP+/mylz2-mCherry-negative* and *myf5-GFP-negative/ mylz2-mCherry+* cells (p < 0.01, Fisher's exact test; Figures 2F–2J). Taken together, our fluorescent transgenic approach identifies unique ERMS cell subpopulations that have different fluorescent reporter expression, divergent gene expression profiles, and varied capacities for proliferation and apoptosis.

myf5-GFP+ Cells Are the ERMS-Propagating Cell Population

To assess if *myf5-GFP* transgene expression enriches for ERMS-propagating potential, cells were isolated from transplant animals that developed *myf5-GFP+/mylz2-mCherry+* ERMS (Figures 3A–3G) and subjected to two rounds of FACS in the

presence of propidium iodide or DAPI to isolate highly purified and viable cells (Figures 3H–3K; 87.7%–99.7% purity and >98% viability). ERMS cell subpopulations were introduced into CG1 syngeneic recipient animals at limiting dilution (Figure 3L–3R), and animals were assessed for engraftment from 10 to 120 days posttransplantation (Table 1). All animals developed ERMS before 45 days posttransplantation, confirming that slower cycling ERMS-propagating cell types would not be missed in our analysis. In three ERMS tumors tested, the tumor-propagating activity was confined to the *myf5-GFP+/mylz2-mCherry-negative* cell subpopulation (Table 1), with an average frequency of 1 in 146 cells capable of reinitiating tumors in recipient animals (range 1 in 87–245, 95% confidence interval). By contrast, only 1 in 4,206 *myf5-GFP+/mylz2-mcherry+* cells were capable of inducing tumors (range 1 in 1,550 to 11,409, 95% confidence interval, p = 3.38e-15 when compared to ERMS-propagating activity in *myf5-GFP+/mylz2-mcherry-negative* cells). Of 61 animals, none
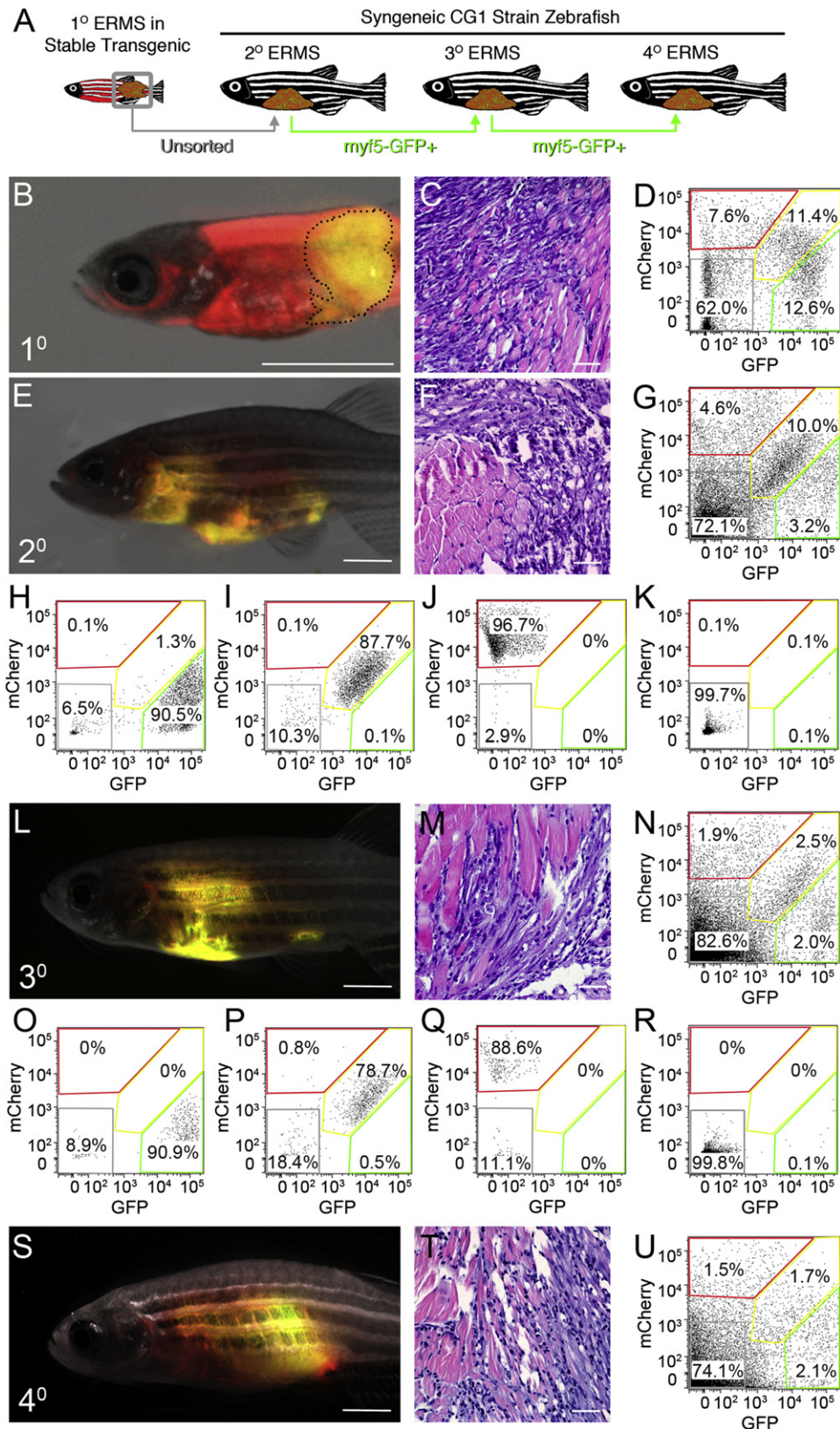
Figure 3. ERMS-Propagating Cells Express *myf5-GFP* but Not the *mylz2-mCherry* Differentiated Muscle Marker
(A) Schematic of experimental design.
(B–D) A primary ERMS arising in syngeneic *myf5-GFP/mylz2-mCherry* transgenic zebrafish (35 dpf). Broken black line denotes tumor area.

Table 1. Limiting Dilution Cell Transplantation Identifies that *myf5-GFP+/mylz2-mCherry-negative* Cells Are the ERMS-Propagating Cells

ERMS #1 2° Transplants					3° Transplants
Cell #	G+	G+R+	R+	Neg	G+
1,000	6 of 6	2 of 7	0 of 6	0 of 7	6 of 6
10	5 of 9	0 of 9	0 of 8	0 of 10	7 of 8
10	0 of 8	0 of 8	0 of 9	0 of 7	0 of 10
TPC #	1 in 140**	1 in 3,461	NA	NA	1 in 67
95% CI	59–329	872–13,740	NA	NA	31–143

ERMS #2 2° Transplants				
Cell #	G+	G+R+	R+	Neg
1,000	6 of 6	0 of 6	0 of 6	0 of 6
10	4 of 7	2 of 10	0 of 10	0 of 10
10	1 of 8	0 of 9	0 of 10	0 of 8
TPC #	1 in 109**	1 in 3,495	NA	NA
95% CI	44–270	808–15,120	NA	NA

ERMS #3 2° Transplants				
Cell #	G+	G+R+	R+	Neg
1,000	2 of 3	0 of 2	0 of 3	0 of 4
10	8 of 9	0 of 8	0 of 8	1 of 8
10	1 of 8	0 of 9	0 of 9	0 of 9
TPC #	1 in 159**	NA	NA	1 in 4,840
95% CI	63–401	NA	NA	632–37,094

Asterisks denote significant differences in tumor-propagating cell number (TPC #) between *myf5-GFP+/mylz2-mCherry-negative* and double-positive ERMS cells (**p < 0.00001). Neg, negative; NA, not applicable; 95% CI, 95% confidence interval.

engrafted disease from terminally differentiated *myf5-GFP-negative/mylz2-Cherry+* cells (lower bound for ERMS-propagating potential was 1 in >5,969 cells). In total, we observed a remarkable 28- to >40-fold enrichment of tumor-propagating potential within our *myf5-GFP+/mylz2-mCherry-negative* cell type when compared with other sorted ERMS cell subpopulations. Similar results were also observed in primary ERMS. Specifically, three primary ERMS tumors were isolated from 20- to 30-day-old larval zebrafish, pooled, and fluorescent-labeled ERMS cell subpopulations were isolated by FACS. Of eight animals, three engrafted disease from 10^2 *myf5-GFP+/mylz2-mCherry-negative* cells, whereas the remaining ERMS cell subpopulations could not transfer disease at this cell dose (0 of 23, purity 83%–98% and viability > 98.6%, p = 0.012, Fisher's exact test). These results further support our finding that the *myf5-GFP+/mylz2-mCherry-negative* population is highly enriched for ERMS-propagating activity.

To assess the long-term tumor-propagating potential of the *myf5-GFP+/mylz2-mCherry-negative* ERMS cells, cells were re-isolated from transplant recipient animals (Figure 3N) and introduced into CG1, syngeneic recipient animals (>78.9% purity and 96% viable; Figures 3O–3R). Again, the *myf5-GFP+/mylz2-mCherry-negative* cell subpopulation was capable of remaking ERMS (Figure 3S–3U; Table 1). Histological analysis showed that primary and serially transplanted ERMS arising from *myf5-GFP+/mylz2-mCherry-negative* cell populations have similar morphology and overall proportions of fluorescent-labeled ERMS cell subpopulations (Figures 3C, 3D, 3F, 3G, 3M, 3N, 3T, and 3U).

Visualizing *myf5-GFP+* ERMS-Propagating Cells In Vivo

To assess whether *myf5-GFP+* ERMS cells could be directly visualized in live animals, *rag2-dsREDexpress* and *rag2-KRASG12D* were coinjected into one-cell-stage *myf5-GFP* transgenic animals and assessed by confocal microscopy. Discrete *myf5-GFP+* tumor cells could be readily identified by confocal imaging with a majority of *myf5-GFP+* ERMS cells coexpressing both GFP and dsREDexpress (97.5 ± 2.9%; n = 568 cells counted in three animals). Moreover, *myf5-GFP+* early muscle progenitor cells from control animals were relatively rare (n = 3 [animals]; 2.3 ± 2.3 cells per imaging field), whereas *myf5-GFP+* cells were abundant in ERMS (n = 3; 194.2 ± 23.7 cells per field, t test, p = 0.0002). Taken together, our data suggest that a vast majority of *myf5-GFP+* cells contained within the boundaries of the ERMS mass are tumor derived.

To further refine the ERMS cell subpopulations for imaging studies, triple fluorescent transgenic ERMS animals were created by microinjecting *myogenin-H2B-RFP*, *mylz2-lyn-cyan*, and *rag2-KRASG12D* into one-cell-stage *myf5-GFP* transgenic animals (Figures 4A–4C). Histone fusion proteins are long lived and confined to the nucleus, whereas *lyn-cyan* encodes for membrane localized blue fluorescent protein. Because transgenes cointegrate as concatamers (Langenau et al., 2008), ERMS cells coexpress all three transgenes and label distinct tumor cell compartments associated with stages of muscle development (Figure S2). In normal development, *myf5* is expressed in satellite cells and early muscle progenitor cells, *myogenin* is expressed in committed, mid-differentiated muscle myoblasts, and *mylz2* is expressed in differentiated myoblasts. Transgenic reporters have been described for all three of these promoters, and each drives expression within the correct cellular compartments during normal muscle development (Chen et al., 2007; Du et al., 2003; Ju et al., 2003). Moreover, gene expression studies confirm that these promoters drive correct tissue-specific gene expression in ERMS (Figure S2), and additional cell transplantation experiments establish that *myf5-GFP+/myogenin-negative* cell types exclusively retain ERMS-propagating potential (Figure S2). For example, 4 of 18 animals engrafted ERMS from 10^2 *myf5-GFP+/myogenin-H2B-RFP-negative* sorted ERMS cells

---

(E–G) Fluorescent-labeled ERMS engraft into syngeneic secondary recipient animals when transplanted with unsorted primary ERMS cells.

(H–K) FACS plots of fluorescent-labeled ERMS cells isolated from secondary recipient fish following two rounds of FACS.

(L–R) Transplantation of *myf5-GFP+/mylz2-mCherry-negative* FACs sorted cells induced ERMS in tertiary transplant animals (L–R) and quaternary recipients (S–U).

Hematoxylin- and eosin-stained sections (C, F, M, and T) and FACS (D, G, N, and U) of primary and serially passaged ERMS. Scale bars, 2 mm (for B, E, L, and S) and 100 μm (for C, F, M, and T).
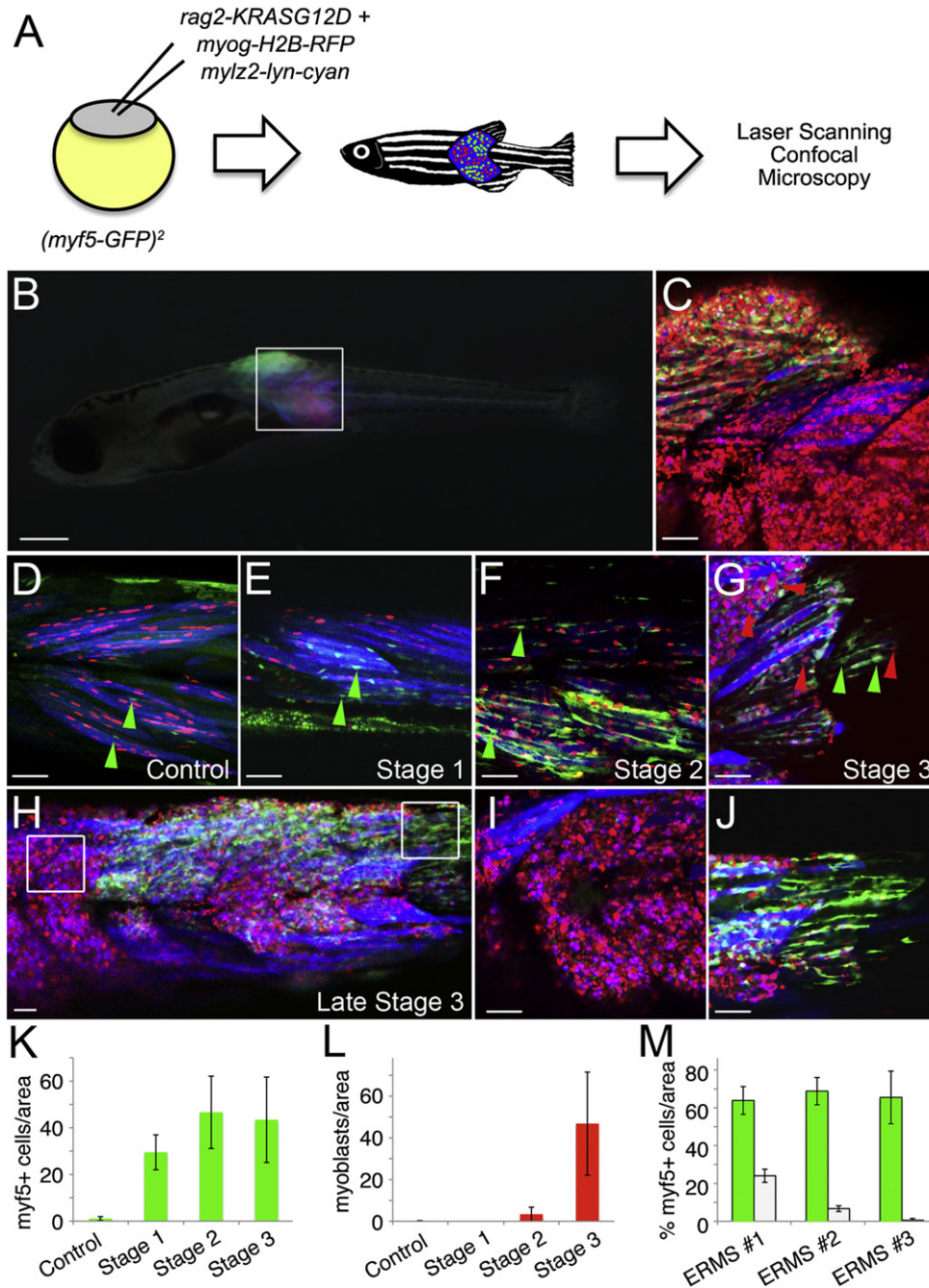
Figure 4. *myf5-GFP*+ ERMS-Propagating Cells Are Dynamically Reorganized during Tumor Growth

(A) Schematic of the experimental design.

(B) A *myf5-GFP* transgenic animal injected at the one-cell stage of life with *rag2-KRASG12D*, *myogenin-H2B-RFP*, and *mylz2-lyn-cyan* with triple fluorescent-labeled ERMS at 16 days of life.

(C) A merged confocal image of the boxed region shown in (B).

(D) Control *myf5-GFP* transgenic animal injected with *myogenin-H2B-RFP* and *mylz2-lyn-cyan*. *myf5-GFP*+ muscle precursor cells are denoted by green arrowheads.

(E–G) Representative image of an ERMS-affected zebrafish labeled with *myf5-GFP*, *myogenin-H2B-RFP*, and *mylz2-lyn-cyan* at stages 1, 2, and 3, respectively. Green arrowheads denote *myf5-GFP*+ cells, whereas red arrowheads denote mononuclear *myogenin-H2B-RFP*+ ERMS cells.

(H) Late stage 3 ERMS from a triple fluorescent-labeled animal.

(I and J) Boxed regions in (H) imaged at higher magnification show regional partitioning of differentiated cells (I) compared with *myf5-GFP*+ ERMS-propagating cells (J).

(K) Quantification of *myf5-GFP*+ cells during stages of ERMS growth when compared to control animals.

(L) Quantification of mononuclear *myogenin-H2B-RFP*+ cells during stages of ERMS growth when compared to control animals.

(68.5% purity, 99.8% viable), whereas *myogenin-H2B-RFP+* cell types could not induce tumors, regardless of whether they expressed *myf5-GFP* (n = 0 of 32, p = 0.013, Fisher's exact test).

Confocal imaging of fluorescent-transgenic ERMS fish that express *myf5-GFP/myogenin-H2B-RFP/mylz2-lyn-cyan* easily identified *myf5-GFP+* cells, of which a small subset coexpress *myogenin-H2B-RFP* (Figure 4C). Some *myogenin-H2B-RFP+* cells with nuclear fluorescent protein expression fail to express either *myf5-GFP* or *mylz2-lyn-cyan*, indicating that these cells are most similar to midmyoblast stages. Gene expression studies confirm that *myogenin*-promoter expression drives H2B-fluorescent protein expression in a subset of myosin-heavy-chain-expressing muscle cell populations, implying that these represent differentiated cell types (Figure S2). Nearly all *mylz2-lyn-cyan+* cells coexpress *myogenin-H2B-RFP* (99.5% ± 1%; n = 8 ERMS, n > 1,700 cells counted), reflecting that H2B-fluorescent protein expression persists in more differentiated ERMS cells.

myf5-GFP+ cells Are Reorganized into Discrete Compartments during Late-Stage Tumor Growth

We next wanted to define the location of ERMS cell subpopulations during various stages of tumor growth. *myf5-GFP* transgenic animals were injected with *rag2-KRASG12D, myogenin-H2B-RFP*, and *mylz2-lyn-cyan* and imaged by confocal microscopy starting at 10 days of life. Stage 1 ERMS exhibited greatly expanded numbers of *myf5-GFP+* cells when compared to control animals and were confined to regions immediately adjacent to muscle fibers (Figures 4D–4G and 4K). Mononuclear *myogenin-H2B-RFP+* and double-positive *myogenin-H2B-RFP+/ mylz2-lyn-cyan+* ERMS cells were not observed in stage 1 ERMS; however, they were detected by stage 2 and increased in number as tumors progressed to stage 3 (Figures 4F–4I and 4L). By late stage 3 ERMS, *myf5-GFP+* cells lost fiber contacts and began to populate discrete portions of the tumor that were physically separated from more differentiated *myogenin-H2B-RFP-* and *mylz2-lyn-cyan*-expressing ERMS cells (Figures 4H–4J and 4M). The *myf5-GFP+* cells were often located within different myotome segments compared to differentiated ERMS cell subpopulations; however, regional partitioning of cells based on differentiation status was also observed within a single myotome segment and in transplanted animals (Figure S2), confirming that compartmentalization did not result from physiological constraints imposed during development but rather was an intrinsic property of ERMS growth.

Human ERMS Cells Are Also Compartmentalized Based on Myogenic Factor Expression

To assess whether human RMS cells also contain distinct regions of tumor cells based on myogenic factor expression, primary human ERMS and xenografted human ERMS derived from RD and SMS-CTR cell lines (Linardic et al., 2005) were assessed for myogenic marker expression, including Myogenin, PAX7, and MYOD. Distinct regions of high and low Myogenin-expressing cells were seen in a vast majority of primary tumor samples (n = 12 of 14, p < 0.03, Student's t test) and were present in all xenograft tumors (n = 7, six regions per tumor, p < 0.02, Students's t test; Figure 5 and Figure S3; Table S2). By contrast, most ARMS cells expressed Myogenin, and its expression was not confined to specific areas within the tumor mass (n = 10; range = 79%–99%), suggesting that regional partitioning of tumor cells based on Myogenin expression is specific to ERMS. We also stained four primary human ERMS tumors for PAX7 and identified regions of high and low expression in two of the four tumors. In one ERMS sample, expression was diffuse while the other tumor was PAX7 negative, indicating that not all primary ERMS cells express PAX7. Unfortunately, MYF5 antibodies have not been developed to detect human protein within paraffin-embedded sections, precluding analysis of less differentiated regions contained within the tumors.

myogenin+ ERMS Cells Are Highly Migratory and Precede the Recruitment of *myf5+* ERMS-Propagating Cells into Newly Colonized Areas of Growth

Having established that the *myf5-GFP*-expressing ERMS cell population contains tumor-propagating activity, we wanted to assess if these cells also promote invasive tumor growth. Multiphoton intravital microscopy recordings from *myf5-GFP/myogenin-H2B-RFP* or *myf5-GFP/myogenin-H2B-Amcyan* transgenic tumor zebrafish revealed that *myf5-GFP+* single-positive ERMS cells were largely stationary and displayed only confined crawling movements (Figures 6A–6F and S4; Movies S2, S3, S4, and S5). In contrast, *myogenin+* ERMS cells were robustly migratory and had the ability to invade across myotome segments through a normally impenetrable collagen matrix. Cells that expressed lower amounts of the H2B-fluorescent fusion protein were orderly arranged along the direction of muscle fibers, had uniform nuclear shape, and did not show any motility (Movies S2 and S3), suggesting that these were differentiated tumor cells of which a subset had undergone fusion (Figure 6F, right).

ERMS cell subpopulations also differ in their proliferative capacity. Primary ERMS cells from *myf5-GFP+/myogenin-H2B-RFP+* animals were pulsed with EDU for 6 hr and then sectioned and assessed for EDU incorporation (Figures 6G–6I). *myf5-GFP+* ERMS cells were highly proliferative (39.4% ± 9.4%; n = 3), whereas *myf5-GFP-negative/myogenin-H2B-RFP+* cells rarely proliferated (2.6% ± 3.8%; n = 3, p = 0.0001). In vivo multiphoton imaging of transplant and primary ERMS confirmed that *myf5-GFP+/mylz2-negative* ERMS-propagating cells are highly proliferative, with 27 of 90 GFP+ cells dividing into two daughter cells (n = 3 tumors). Multiphoton imaging revealed that resting *myf5-GFP+* ERMS cells are elongated (Figure 6J) and then round up in shape just prior to cell division (Figure 6K). Following this dynamic shape change, *myf5-GFP+* ERMS cells quickly divide

---

(M) Quantification of regional compartmentalization of ERMS cells based on differentiation status in late stage 3 tumors (n = 3). Green bars denote regions that contain higher percentages of *myf5-GFP+* ERMS-propagating cells compared to white bars where *myf5-GFP+* cells are less abundant and conversely more differentiated.

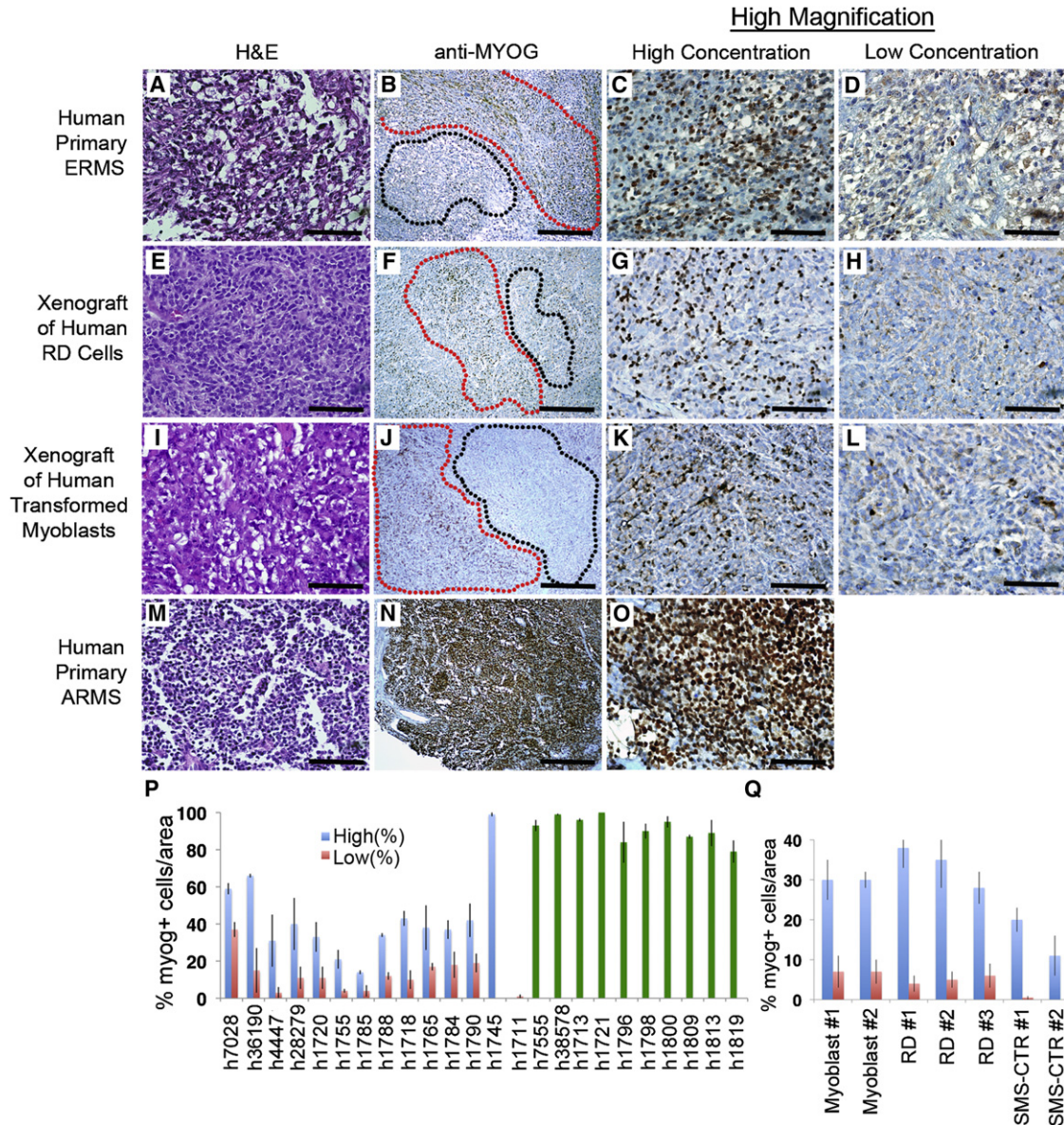Error bars in (K–M), ±1 SD. Scale bar, 500 μm for (B) and 50 μm for (C–J).

See also Figure S2.

Figure 5. Human Embryonal RMS Exhibit Regional Portioning of Cells Based on Myogenic Factor Expression

(A–D) Primary human ERMS.

(E–L) RD human cell lines (E–H) or human RAS-transformed myoblasts (I–L) introduced into SCID/*beige* mice.

(M–O) Primary human ARMS. Hematoxylin/Eosin-stained sections (A, E, I, and M) and anti-Myogenin immunohistochemistry performed on adjacent sections (B, F, J, and N). Regions containing high numbers of Myogenin+ cells are denoted by red outline, while regions with low numbers of Myogenin+ cells are denoted by black outline (B, F, and J). ARMS did not show regional portioning based on Myogenin staining (N). Magnified views of areas with high concentrations of Myogenin+ cells (C, G, K, and O) or areas with low or absent expression (D, H, and L).

(P–Q) Quantification of regional compartments in primary and metastatic human RMS (P) and in mice xenografted with human RD and SMS-CTR ERMS cells and human RAS-transformed myoblasts (myoblasts, in Q). Numbers in (Q) denote tumors arising in separate animals. Blue bars denote areas with high percentages of Myogenin+ cells compared to areas with low numbers of cells (red bars). Green bars denote diffuse and ubiquitous expression of Myogenin within ARMS. Error bars, ±1 SD. Scale bars, 50 μm (for A, C–E, G–I, K–M, and O) and 200 μm (for B, F, J, and N).

See also Figure S3 and Table S2.

into two GFP-labeled daughter cells (Figures 6L–6M). Subsequently, these daughter cells begin to reacquire parental morphology (Movie S6), reminiscent of normal *myf5-GFP+* muscle precursors. By contrast, 0 of 90 *mylz2+* cells proliferated over this time, regardless of whether they expressed *myf5-GFP*.

To further visualize the dynamic movements of ERMS cells in vivo, late stage 3 triple transgenic ERMS affected animals were serially imaged over 16 hr to capture cell movements (Figures 7A–7H; Movie S7). As was seen in our multiphoton imaging, *myf5-GFP+* cells that lack differentiated marker
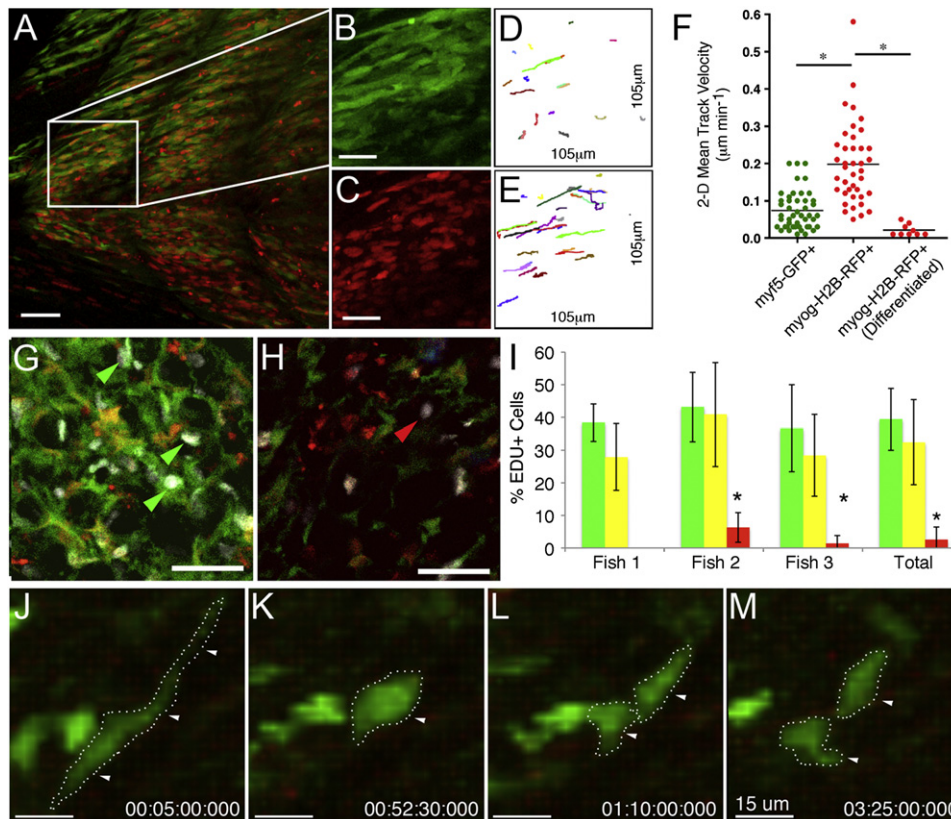
Figure 6. *myf5-GFP*+ ERMS-Propagating Cells Are Slow Moving but Highly Proliferative while *myogenin-H2B-RFP*+ Cells Do Not Divide but Are Highly Migratory

(A–E) Multiphoton recording of a stage 3 ERMS arising in *myf5-GFP/myogenin-H2B-RFP* transgenic zebrafish (B and C) Magnified view of the boxed region in (A) showing *myf5-GFP*+ (B) or *myogenin-H2B-RFP*+ ERMS cells (C).

(D and E) Tracks of cell movement over the 6.7-hr observation period. The same areas are shown as in (B) and (C), respectively.

(F) Mean track velocities of representative cell types contained within the tumor mass. *p < 0.001.

(G and H) EDU staining of double transgenic *myf5-GFP+/myogenin-H2B-RFP*+ primary zebrafish ERMS (35 dpf). Confocal image of a tumor section with high numbers of *myf5-GFP*+ ERMS cells (G) compared to a section with high numbers of *myogenin-H2B-RFP*+ cells (H). White denotes nuclei that have incorporated EDU. EDU incorporation into *myf5-GFP*+ or *myogenin-H2B-RFP*+ ERMS cells denoted by green or red arrows, respectively.

(I) Quantification of proliferation over the 6 hr EDU pulse. *myf5-GFP+/myogenin-H2B-RFP-negative* (green bars), double positive (yellow bars), and *myf5-GFP-negative/ myogenin-H2B-RFP*+ (red bars). Error bars, ±1 SD. Asterisk denotes significant differences, *p = 0.0001.

(J–M) Static images of a *myf5-GFP*+ ERMS cells dividing. Scale bars, 50 μm (for A, G, and H), 25 μm (for B–E), and 15 μm (for J–M).

See also Figure S4 and Movies S2, S3, S4, S5, and S6.

expression move only locally within the tumor and exhibit regional crawling movements, whereas *myogenin-H2B-RFP+/ mylz2-lyn-cyan-negative* cells are highly motile and could be easily visualized migrating into adjacent nonaffected normal tissue (Figures 7A–7D; Movie S7). By contrast, differentiated ERMS cells that express *myogenin-H2B-RFP* and *mylz2-lyn-cyan* are largely stationary.

To investigate which ERMS cells were the first to migrate into unaffected tissue, we conducted serial imaging experiments over longer observation intervals, focusing on regions that were adjacent to expanding tumor. Serial confocal imaging of fluorescent ERMS fish over several days revealed that *myogenin-H2B*+ ERMS cells precede the recruitment of *myf5-GFP*+ cells into newly colonized areas of tumor growth (n = 7; Figures 7I, 7J, and S4). Not only do fluorescent-labeled *myogenin-H2B*+ ERMS cells move locally within the tumor, but they also

enter the vasculature (Movie S8). A small portion of *myogenin-H2B-RFP+/myf5-GFP-negative* cells were associated with vasculature and could invade neovascular beds in *fli1-GFP* transgenic animals (Figures 7K and 7L). To verify the fidelity of H2B-fluorescent labeling of ERMS cell subfractions and to directly visualize if *myf5-GFP*+ ERMS cells can enter the vasculature, we induced ERMS in stable transgenic animals that express *myf5-GFP/flk1-mCherry* by coinjecting both *rag2-KRASG12D* and *myogenin-H2B-Amcyan*. As was seen using the H2B-RFP transgenic reporter, we found that *myogenin-H2B-Amcyan*+ cells are highly migratory (Movies S4 and S5), were the first cell type to colonize new areas of tumor growth, and could be observed transiting the vasculature (Figures 7M and 7N; Movies S5 and S9). By contrast, *myf5-GFP*+ ERMS cells exhibited reduced motility when compared with *myogenin*+ ERMS cells and were never observed entering the vasculature
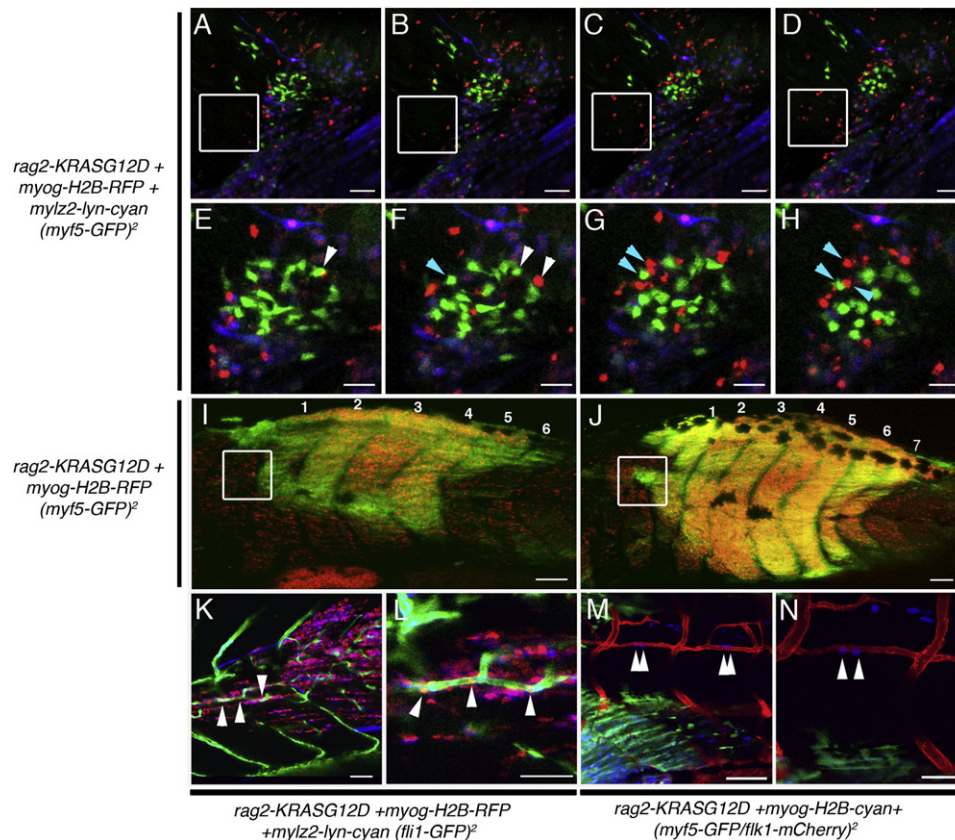
Figure 7. *myf5-GFP*+ ERMS-Propagating Cells Are Recruited to New Areas of Tumor Growth Only after Seeding by *myogenin*+ ERMS Cells
(A–H) Time-lapse images of *myf5-GFP* transgenic animal injected with *rag2-KRASG12D, myogenin-H2B-RFP* and *mylz2-lyn-cyan*. Panels are merged image planes taken every hour. *myogenin-H2B-RFP*+ cells migrate into normal tissues over time (white boxed region). Magnified views of time-lapse images documenting that *myf5-GFP*+ cells are largely stationary while *myogenin-H2B-RFP*+ cells are highly migratory and migrate away from GFP+ cells (denoted by arrows in E–H).
(I and J) Serial imaging of a *myf5-GFP* transgenic animal injected with *rag2-KRASG12D* and *myogenin-H2B-RFP* shown at 14 and 17 dpf, respectively. White boxes denote a region that initially contained only *myogenin-H2B-RFP*+ cells (I) but was later colonized by *myf5-GFP*+ cells (J).
(K and L) ERMS developing in a *fli1-GFP* transgenic animal injected with *rag2-KRASG12D, myogenin-H2B-RFP,* and *mylz2-lyn-cyan*. (K) Merged z-stacks showing three *myogenin-H2B-RFP*+ cells associated with and inside *fli1-GFP*+ vessels, which was confirmed by imaging a single image plane at higher magnification (L, white arrowhead).
(M and N) ERMS developing in a *flk1-mCherry* transgenic animal injected with *rag2-KRASG12D* and *myogenin-H2B-cyan* showing four cells entering the vasculature (white arrowheads in M) and a single plane image showing two cells transiting into the vasculature at higher magnification (white arrowheads in N). Scale bar, 50 μm (for A–H, K, L, and N) and 100 μm (for I, J, M).
See also Figure S4 and Movies S7, S8, and S9.

(n = 10 animals). Again, slow-moving *myf5-GFP*+ cells were found in newly colonized regions only after initial invasion by *myogenin*+ ERMS cells.

DISCUSSION

Myf5 as a Marker of ERMS-Propagating Cells
The limiting dilution cell transplantation studies outlined here confirm the existence of a highly purified and molecularly definable ERMS-propagating cell that expresses *myf5*, *m-cadherin*, and *c-met* but not differentiated muscle markers. The *myf5-GFP*+ ERMS-propagating cell gives rise to all the other differentiated ERMS cells contained within the tumor mass and exhibits enhanced proliferative capacity as assessed by EDU incorporation and direct in vivo cell imaging. These results are in keeping

with our previous work showing that ERMS-propagating activity was largely confined to the *rag2-dsRED+/α-actin-negative* ERMS cell population that preferentially expressed *myf5* and other activated satellite cell markers (Langenau et al., 2007). However, *rag2-dsRED+/α-actin-negative* ERMS cells exhibited only a modest 3-fold enrichment for tumor-propagating potential when compared to *rag2-dsRED+/alpha-actin+* ERMS cells (Langenau et al., 2007). By contrast, experiments outlined here using new fluorescent transgenic reporter lines and syngeneic zebrafish show that the *myf5-GFP+/mylz2-negative* ERMS cells exhibit a remarkable 28- to >40-fold enrichment of tumor-propagating potential when compared to other ERMS-derived cell populations.

Myf5 is a myogenic regulatory factor related to MyoD and has important roles in muscle development. For example,

MyoD/Myf5-deficient mice lack muscle, while deficiencies in only one of these genes does not affect muscle specification (Rudnicki et al., 1993), suggesting important and yet redundant functions of these genes in development. It has also been shown that *Myf5* is highly expressed in activated satellite cells and has important roles in postnatal muscle regeneration in response to injury (Cooper et al., 1999; Gayraud-Morel et al., 2009; Ustanina et al., 2007), suggesting that Myf5 may regulate self-renewal in normal muscle satellite cells. Microarray analysis and cross-species comparisons have shown that *MYF5* is upregulated in both zebrafish and human ERMS but not translocation-positive ARMS (Langenau et al., 2007; Zibat et al., 2010), and recent work from Rubin et al. (2011) has shown that *Myf5* is differentially expressed in murine ERMS regardless of which muscle cell subpopulation is initially targeted for transformation. These results suggest that *Myf5* gene programs are likely reinitiated in transformed cells and may have important roles in driving ERMS growth. By contrast, translocation-positive ARMS fail to express *MYF5*, precluding *MYF5* marker expression as an identifying characteristic of ARMS-propagating cells and raising the interesting possibility that the molecular mechanisms regulating tumor-propagating potential differ between molecular subtypes of RMS. Given the critical roles of the Myf5 transcription factor in muscle development and regeneration in mice, it will be important to assess if *myf5* is a marker of ERMS-propagating cells or if it plays a regulatory role in ERMS self-renewal and growth.

Regional Partitioning of ERMS Cells Based on Differentiation Status

Evidence in solid tumors to support a discrete, specialized microenvironment that augments tumor growth and proliferation is now just beginning to emerge. For example, tumor-propagating cells, including those of glioblastomas, have been shown to reside in a vascular niche that promotes both their maintenance and their ability to divide and produce daughter cells capable of inducing tumors (reviewed by Gilbertson and Rich, 2007). In other solid tumors arising in skin, prostate, and breast, tumor stromal fibroblasts also serve an essential role in maintaining a favorable microenvironment for tumor growth and expansion. For example, work by Orimo et al. (2005) has shown that stromal fibroblasts associated with invasive breast carcinoma cells can promote tumor growth and angiogenesis through secretion of SDF-1. In normal muscle, stem cell numbers are exquisitely regulated by paracrine factors like Wnt5a (Polesskaya et al., 2003), Myostatin (McCroskery et al., 2003), and Notch ligands (Conboy et al., 2003). Many of these factors are secreted by normal fibers that can sense injury and elicit recruitment and expansion of muscle progenitors that are required for regeneration. Thus, mature muscle provides a supportive microenvironment that facilitates homeostatic regulation of muscle stem cells. In our zebrafish ERMS model, we document that *myf5-GFP*+ ERMS-propagating cells are initially juxtaposed to muscle fibers in an expanded muscle satellite/progenitor cell niche, suggesting that early stage ERMS cells cannot escape the constraints of muscle architecture or are held in check by local secreted factors emanating from normal muscle. By the late stages of ERMS growth, ERMS-propagating cells are reorganized and take up residence in defined regions within the tumor mass. Following this regional partitioning of ERMS cells,

mid-differentiated *myogenin*+ ERMS cells show enhanced migratory capability and move away from the ERMS-propagating cells from which they had arisen. These mid-differentiated myogenin+ ERMS cells are highly migratory, seed new areas of tumor growth, and cease to move once they turn on differentiated muscle markers including muscle myosin light chain. Such biologically constrained characteristics of ERMS cells would ensure that tumor-propagating cells remain confined to regionally defined areas and do not compete with differentiated ERMS cells for local resources including growth factors and oxygen. The extent to which regional partitioning of tumor cells occurs in other solid tumors is unknown; however, assuming this phenomenon is found in diverse cancer types, it will be important to determine if regional partitioning of tumor cells provides protective advantages to tumor-propagating cells, facilitating the retention of a small number of cancer cells that evade treatment and eventually give rise to disease relapse.

A Role for Differentiated, Non-Tumor-Propagating Cells in Facilitating Tumor Growth and Metastasis

Myogenin immunohistochemical reactivity found in >80% of RMS cells distinguishes patients with poor clinical outcome (Heerema-McKenney et al., 2008), suggesting that *Myogenin*+ cells have a unique role in RMS progression and metastasis. In our model, *myogenin-H2B*+ cells arise from *myf5-GFP*+ ERMS-propagating cells, lack tumor-propagating potential, and are the first cell type to migrate into new areas of tumor growth. A subset of *myogenin*+ ERMS cells infiltrate blood vessels—a first step toward metastasis—and are also the first to colonize new areas of tumor growth, only to be infiltrated later by slow-migrating *myf5*+ ERMS-propagating cells. Our work raises the interesting possibility that differentiated, non-ERMS-propagating cells may create a supportive environment that augments growth and is responsible for local tumor invasion. For example, it is possible that once mid-differentiated *myogenin*+ cells infiltrate new areas of growth, that they secrete factors that recruit slow-moving *myf5*+ ERMS-propagating cells, facilitating tumor spread. Alternatively, it is possible that *myogenin*+ cells break down collagen and cell-cell contacts, acting as trailblazers to establish migratory tracks that allow slow-moving *myf5*+ ERMS-propagating cells to transit into newly forming tumor. Our work also highlights that metastatic capacity and tumor-propagating potential need not be confined to the same tumor cell subpopulations, but rather that local infiltration and metastasis may be facilitated by differentiated, non-tumor-propagating cells. We expect that these same principles may be more broadly applicable to a diversity of cancers, accounting for why tumors retain large numbers of differentiated cell types that themselves are incapable of reconstituting tumor.

Our findings of a *myf5*+ ERMS-propagating cell population and a *myogenin*+ migratory population both contributing to tumorigenesis may have profound therapeutic implications. Instead of targeting only tumor-propagating cells for destruction, drug design should also take into account the mechanisms regulating the homeostasis of more differentiated tumor cells and their nonproliferative roles in regulating growth. Moreover, therapies that focus on modulating the differentiation status of ERMS cells should attempt to force the conversion of tumor-propagating cells into cells with terminally differentiated

myoblast characteristics that are incapable of recreating tumor, cannot migrate, and fail to enter into the vasculature.

EXPERIMENTAL PROCEDURES

Study Approval

These studies were approved by the Massachusetts General Hospital Subcommittee on Research Animal Care under protocol #2011N000127 (zebrafish), the Duke University Institutional Animal Care & Use Committee under protocol A 036-03-02 (mouse), and the Partners Human Research Committee under protocol #2009-P-002756 (human). Samples were obtained from the Pathology Department of Massachusetts General Hospital. Use of decoded, paraffin-embedded human tissue samples does not require informed consent.

Animals

CG1-strain (Smith et al., 2010), α-actin-GFP (Higashijima et al., 1997), myf5-GFP (Chen et al., 2007), fli1-GFP (Lawson and Weinstein, 2002), flk1-mCherry (Wang et al., 2010), and mylz2-mCherry transgenic zebrafish (Smith et al., 2010) have been reported previously.

The rag2-KRASG12D, rag2-dsREDexpress, myogenin-H2B-RFP, myogenin-H2B-Amcyan, and mylz2-lyn-cyan constructs were microinjected into one-cell-stage zebrafish singly (rag2-KRASG12D injected into myf5-GFP/mylz2-mCherry syngenic zebrafish, 60 ng/μl) or as combinations with linearized DNA at a final combined concentration of 120 ng/μl essentially as described (Langenau et al., 2008).

FACS and ERMS Cell Transplantation

FACS analysis and ERMS cell transplantation were completed essentially as described elsewhere (Smith et al., 2010; Langenau et al., 2007). Sort gates were placed based on wild-type control fish and myf5-GFP+, mylz2-mCherry+, or mylz2-lyn-cyan+ ERMS. DAPI, propidium iodide, or TOPRO3 was used to isolate viable cells. ERMS tumors were double sorted to obtain pure, viable cell populations. Sort purity was assessed after two rounds of sorting when possible. Following limiting dilution cell transplantation into nonirradiated syngeneic CG1-recipient animals, fish were analyzed for fluorescent tumor engraftment from 10 to 120 days posttransplantation. Tumor-propagating potential was quantified using the Extreme Limiting Dilution Analysis software (http://bioinf.wehi.edu.au/software/elda/). A subset of transplanted fish was sectioned and stained with hematoxylin and eosin to confirm the presence or absence of ERMS.

Immunohistochemistry, EDU Staining, and Annexin V Staining

Paraffin embedding and sectioning, cryostat sectioning, and immunohistochemical analysis were performed essentially as described elsewhere (Langenau et al., 2007; see also Supplemental Experimental Procedures). EDU staining was performed using the Click-iT Alexa Fluor 647 imaging kit (Invitrogen). Annexin analysis for apoptotic cells was performed via FACS using annexin V conjugated to Alexa Fluor 647 (Invitrogen).

Gene Expression Analysis

Total RNA was isolated from AB-strain embryos 6 and 24 hr postfertilization and FAC-sorted ERMS cell subpopulations (TRIzol, GIBCO/BRL) in the presence of glycol blue. Quantitative real-time PCR utilized gene-specific PCR primers (Supplemental Experimental Procedures), and expression was normalized to 18 s and β-actin controls to obtain relative transcript levels using the $2^{-\Delta\Delta CT}$ method. Relative gene expression was normalized within individual samples, and cumulative transcript expression across the four ERMS cell subpopulations was set to 25. Samples were assessed in relation to embryos 6 and 24 hr postfertilization to ensure that results for $2^{-\Delta\Delta CT}$ results for any given gene were not lower than 10-fold expression found in normal development. Microarray experiments were completed essentially as described (fold change cutoff > 1.5-fold log scale; Langenau et al., 2007). Microarray data have been deposited into the GEO database (GSE32425).

Laser Scanning Confocal Microscopy and Dual Photon Imaging

Larval zebrafish were anesthetized in Tricaine and embedded in a single drop of low melt 1% agarose on a glass bottom petri dish (No 1.5, Mat Tek Corporation). Each petri dish was supplemented with fish water and imaged using an inverted Pascal or LSM510 Zeiss laser scanning confocal microscope or an upright Ultima IV multiphoton microscope (Prairie Technologies). Quantification was completed by counting the total numbers of fluorescent-labeled ERMS cell subpopulations contained in two 250 × 150 μm areas per animal (Figures 4K and 4L; control, n = 7; stage 1, n = 3; stage 2, n = 4; stage 3, n = 7). Because regional niches can be compartmentalized within a single myotome segment, a smaller area was assessed for total numbers of myf5-GFP+ and myogenin-H2B-RFP+ ERMS cells (50 × 50 μm^2 area, six areas per tumor; Figure 4M).

For cell tracking, sequences of image stacks were transformed into maximum intensity-projected movies using Imaris 7.1 software (Bitplane) and exported as Quicktime movies. Manual two- or three-dimensional tracking was performed using the manual tracking plugin in ImageJ or using Imaris 7.1. Annotation and further processing of movies was completed using ImageJ and Quicktime 7.

SUPPLEMENTAL INFORMATION

Supplemental Information includes nine movies, two tables, four figures, and Supplemental Experimental Procedures and can be found with this article online at doi:10.1016/j.ccr.2012.03.043.

REFERENCES

Bentzinger, C.F., Wang, Y.X., and Rudnicki, M.A. (2012). Building muscle: molecular regulation of myogenesis. Cold Spring Harb. Perspect. Biol. 4, 4.

Chen, Y.H., Wang, Y.H., Chang, M.Y., Lin, C.Y., Weng, C.W., Westerfield, M., and Tsai, H.J. (2007). Multiple upstream modules regulate zebrafish myf5 expression. BMC Dev. Biol. 7, 1.

Conboy, I.M., Conboy, M.J., Smythe, G.M., and Rando, T.A. (2003). Notch-mediated restoration of regenerative potential to aged muscle. Science 302, 1575–1577.

Cooper, R.N., Tajbakhsh, S., Mouly, V., Cossu, G., Buckingham, M., and Butler-Browne, G.S. (1999). In vivo satellite cell activation via Myf5 and MyoD in regenerating mouse skeletal muscle. J. Cell Sci. 112, 2895–2901.

Dalerba, P., Cho, R.W., and Clarke, M.F. (2007). Cancer stem cells: models and concepts. Annu. Rev. Med. 58, 267–284.

Du, S.J., Gao, J., and Anyangwe, V. (2003). Muscle-specific expression of myogenin in zebrafish embryos is controlled by multiple regulatory elements in the promoter. Comp. Biochem. Physiol. B Biochem. Mol. Biol. 134, 123–134.

Eyler, C.E., Wu, Q., Yan, K., MacSwords, J.M., Chandler-Militello, D., Misuraca, K.L., Lathia, J.D., Forrester, M.T., Lee, J., Stamler, J.S., et al. (2011). Glioma stem cell proliferation and tumor growth are promoted by nitric oxide synthase-2. Cell 146, 53–66.

Gayraud-Morel, B., Chrétien, F., and Tajbakhsh, S. (2009). Skeletal muscle as a paradigm for regenerative biology and medicine. Regen. Med. 4, 293–319.

Gilbertson, R.J., and Rich, J.N. (2007). Making a tumour's bed: glioblastoma stem cells and the vascular niche. Nat. Rev. Cancer 7, 733–736.

Heerema-McKenney, A., Wijnaendts, L.C., Pulliam, J.F., Lopez-Terrada, D., McKenney, J.K., Zhu, S., Montgomery, K., Mitchell, J., Marinelli, R.J., Hart, A.A., et al. (2008). Diffuse myogenin expression by immunohistochemistry is an independent marker of poor survival in pediatric rhabdomyosarcoma: a tissue microarray study of 71 primary tumors including correlation with molecular phenotype. Am. J. Surg. Pathol. 32, 1513–1522.

Hettmer, S., Liu, J., Miller, C.M., Lindsay, M.C., Sparks, C.A., Guertin, D.A., Bronson, R.T., Langenau, D.M., and Wagers, A.J. (2011). Sarcomas induced in discrete subsets of prospectively isolated skeletal muscle cells. Proc. Natl. Acad. Sci. USA 108, 20002–20007.

Higashijima, S., Okamoto, H., Ueno, N., Hotta, Y., and Eguchi, G. (1997). High-frequency generation of transgenic zebrafish which reliably express GFP in whole muscles or the whole body by using promoters of zebrafish origin. Dev. Biol. 192, 289–299.

Ju, B., Chong, S.W., He, J., Wang, X., Xu, Y., Wan, H., Tong, Y., Yan, T., Korzh, V., and Gong, Z. (2003). Recapitulation of fast skeletal muscle development in zebrafish by transgenic expression of GFP under the mylz2 promoter. Dev. Dyn. 227, 14–26.

Keller, C., Arenkiel, B.R., Coffin, C.M., El-Bardeesy, N., DePinho, R.A., and Capecchi, M.R. (2004). Alveolar rhabdomyosarcomas in conditional Pax3:Fkhr mice: cooperativity of Ink4a/ARF and Trp53 loss of function. Genes Dev. 18, 2614–2626.

Langenau, D.M., Keefe, M.D., Storer, N.Y., Guyon, J.R., Kutok, J.L., Le, X., Goessling, W., Neuberg, D.S., Kunkel, L.M., and Zon, L.I. (2007). Effects of RAS on the genesis of embryonal rhabdomyosarcoma. Genes Dev. 21, 1382–1395.

Langenau, D.M., Keefe, M.D., Storer, N.Y., Jette, C.A., Smith, A.C., Ceol, C.J., Bourque, C., Look, A.T., and Zon, L.I. (2008). Co-injection strategies to modify radiation sensitivity and tumor initiation in transgenic Zebrafish. Oncogene 27, 4242–4248.

Lawson, N.D., and Weinstein, B.M. (2002). In vivo imaging of embryonic vascular development using transgenic zebrafish. Dev. Biol. 248, 307–318.

Li, Z., Bao, S., Wu, Q., Wang, H., Eyler, C., Sathornsumetee, S., Shi, Q., Cao, Y., Lathia, J., McLendon, R.E., et al. (2009). Hypoxia-inducible factors regulate tumorigenic capacity of glioma stem cells. Cancer Cell 15, 501–513.

Linardic, C.M., Downie, D.L., Qualman, S., Bentley, R.C., and Counter, C.M. (2005). Genetic modeling of human rhabdomyosarcoma. Cancer Res. 65, 4490–4495.

Lo Celso, C., Fleming, H.E., Wu, J.W., Zhao, C.X., Miake-Lye, S., Fujisaki, J., Côté, D., Rowe, D.W., Lin, C.P., and Scadden, D.T. (2009). Live-animal tracking of individual haematopoietic stem/progenitor cells in their niche. Nature 457, 92–96.

McCroskery, S., Thomas, M., Maxwell, L., Sharma, M., and Kambadur, R. (2003). Myostatin negatively regulates satellite cell activation and self-renewal. J. Cell Biol. 162, 1135–1147.

Orimo, A., Gupta, P.B., Sgroi, D.C., Arenzana-Seisdedos, F., Delaunay, T., Naeem, R., Carey, V.J., Richardson, A.L., and Weinberg, R.A. (2005). Stromal fibroblasts present in invasive human breast carcinomas promote tumor growth and angiogenesis through elevated SDF-1/CXCL12 secretion. Cell 121, 335–348.

Polesskaya, A., Seale, P., and Rudnicki, M.A. (2003). Wnt signaling induces the myogenic specification of resident CD45+ adult stem cells during muscle regeneration. Cell 113, 841–852.

Rubin, B.P., Nishijo, K., Chen, H.I., Yi, X., Schuetze, D.P., Pal, R., Prajapati, S.I., Abraham, J., Arenkiel, B.R., Chen, Q.R., et al. (2011). Evidence for an unanticipated relationship between undifferentiated pleomorphic sarcoma and embryonal rhabdomyosarcoma. Cancer Cell 19, 177–191.

Rudnicki, M.A., Schnegelsberg, P.N., Stead, R.H., Braun, T., Arnold, H.H., and Jaenisch, R. (1993). MyoD or Myf-5 is required for the formation of skeletal muscle. Cell 75, 1351–1359.

Seger, C., Hargrave, M., Wang, X., Chai, R.J., Elworthy, S., and Ingham, P.W. (2011). Analysis of Pax7 expressing myogenic cells in zebrafish muscle development, injury, and models of disease. Dev. Dyn. 240, 2440–2451.

Sipkins, D.A., Wei, X., Wu, J.W., Runnels, J.M., Côté, D., Means, T.K., Luster, A.D., Scadden, D.T., and Lin, C.P. (2005). In vivo imaging of specialized bone marrow endothelial microdomains for tumour engraftment. Nature 435, 969–973.

Smith, A.C., Raimondi, A.R., Salthouse, C.D., Ignatius, M.S., Blackburn, J.S., Mizgirev, I.V., Storer, N.Y., de Jong, J.L., Chen, A.T., Zhou, Y., et al. (2010). High-throughput cell transplantation establishes that tumor-initiating cells are abundant in zebrafish T-cell acute lymphoblastic leukemia. Blood 115, 3296–3303.

Ustanina, S., Carvajal, J., Rigby, P., and Braun, T. (2007). The myogenic factor Myf5 supports efficient skeletal muscle regeneration by enabling transient myoblast amplification. Stem Cells 25, 2006–2016.

Wang, Y., Kaiser, M.S., Larson, J.D., Nasevicius, A., Clark, K.J., Wadman, S.A., Roberg-Perez, S.E., Ekker, S.C., Hackett, P.B., McGrail, M., and Essner, J.J. (2010). Moesin1 and Ve-cadherin are required in endothelial cells during in vivo tubulogenesis. Development 137, 3119–3128.

Xia, S.J., Pressey, J.G., and Barr, F.G. (2002). Molecular pathogenesis of rhabdomyosarcoma. Cancer Biol. Ther. 1, 97–104.

Zibat, A., Missiaglia, E., Rosenberger, A., Pritchard-Jones, K., Shipley, J., Hahn, H., and Fulda, S. (2010). Activation of the hedgehog pathway confers a poor prognosis in embryonal and fusion gene-negative alveolar rhabdomyosarcoma. Oncogene 29, 6323–6330.